Original article

Synthesis, spectroscopic characterization, thermal analysis and *in vitro* bioactivity studies of the *N*-(cinnamylidene) tryptophan Schiff base

Mohammed Mansour S. Saif [a], Riad M. Alodeni [a], Abdulaziz Ali Alghamdi [b], Abdel-Basit Al-Odayni [c,*]

[a] *Division of Biochemistry, Chemistry Department, Faculty of Science, Ibb University, Ibb, Yemen*
[b] *Chemistry Department, College of Science, King Saud University, P.O. Box 2455, Riyadh 11451, Saudi Arabia*
[c] *Engineer Abdullah Bugshan Research Chair for Dental and Oral Rehabilitation, College of Dentistry, King Saud University, Riyadh 11545, Saudi Arabia*

ARTICLE INFO

ABSTRACT

The objective of this study was to investigate the bioactivity of *N*-(cinnamylidene) tryptophan (CinTrp), including its *in vitro* hemolytic effect on erythrocytes, at different concentrations (20–1000 µg/mL). CinTrp was synthesized by condensing cinnamaldehyde (Cin) and tryptophan (Trp) in a basic medium. Its physicochemical, spectral, and thermal properties were analyzed using Fourier transform infrared, proton and 13-carbon nuclear magnetic resonance, electronic, and mass spectroscopy, as well as thermogravimetric and differential scanning calorimetry. Antibacterial activity against Gram-positive (*S. aureus*) and Gram-negative (*E. coli*, *P. aeruginosa*, and *K. pneumoniae*) bacteria was assessed using the agar disk-diffusion method, while the hemolytic effect on human erythrocytes was spectrophotometrically determined. Thermal analysis suggested that CinTrp is less stable than its Trp precursor. The antibacterial activity of CinTrp against *E. coli* was close to that of ceftriaxone, while against *K. pneumoniae* it was nearly half that for ampicillin and ceftriaxone standard drugs. No effects on *S. aureus* and *P. aeruginosa* were observed. Cell hemolysis test in reference to phosphate-buffered saline (negative) and Triton X-100 (0.1% v/v) (positive) controls indicated low or no effects up to 250 µg/mL ($\leq 1.50\% \pm 3.06\%$), with a slight increase up to 750 µg/mL ($6.50\% \pm 2.87\%$); however, lysis of $23.13\% \pm 7.76\%$ at 1000 µg/mL was detected. It could be concluded that CinTrp is more active against Gram-negative bacteria and its hemolytic effect on erythrocytes apparently begins above 250 µg/mL. However, additional analyses in terms of the concentration range, methods, and types of microorganisms may be necessary to assuage safety concerns and deepen understanding.

1. Introduction

Schiff bases are an important class of bioactive compounds that have been extensively studied in the fields of medicinal, organic, and inorganic chemistry. They contain an azomethine linkage, which substantially enhances certain biological activities (Zong Chin et al., 2020). Schiff bases are typically the condensation product of a carbonyl group (aldehyde or ketone) with primary amines. They exhibit a wide range of biological activities, including antipyretic, antimalarial, antiproliferative, antiviral, antitumor, antioxidant, antibacterial, and antifungal effects (Al-Resayes et al., 2020; Alam et al., 2012; Azam et al., 2021a; Khan et al., 2021; Rehman et al., 2013; Zhang et al., 2011). Hence, an in-depth investigation of their structure–property-activity relationship becomes of special interest to researchers.

Cinnamaldehyde (Cin), a major constituent of cinnamon essential oil, is a well-established natural antimicrobial substance that is categorized as a safe compound for use in medicine and food (Adabiardakani et al., 2012). Furthermore, it is non-toxic on human erythrocytes at low concentration (<30 µg/mL) as compared with negative control (da Nóbrega Alves et al., 2020). Despite its distinctive structure, properties such as volatility and strong odor limit its use in many applications (Li et al., 2008). To overcome such disadvantages, various Cin-based derivatives, including Schiff bases, have been synthesized (Li et al., 2008; Shreaz et al., 2011). Cin is a conjugated aromatic aldehyde that can easily react with an

* Corresponding author.
E-mail addresses: md_phd07@yahoo.com (M.M.S. Saif), riadalodeni@gmail.com (R.M. Alodeni), aalghamdia@ksu.edu.sa (A.A. Alghamdi), aalodayni@ksu.edu.sa (A.-B. Al-Odayni).
Peer review under responsibility of King Saud University.

amino group under mild conditions (Wang et al., 2017; Wang et al., 2018), resulting in an emerging class of bioactive compounds with potential application as pharmaceutical agents (Wang et al., 2017). Tryptophan (Trp), an essential amino acid, is the unique protein amino acid bearing an indole, a bicyclic ring formed by a benzene and pyrrole group, providing the molecule with high hydrophobic features among all protein amino acids. Also, the indole ring can be metabolized into bioactive compounds those having a great impact on life functions (Shakir et al., 2011). It is a building block of many substantial biomolecules. In addition, it is an important precursor of pharmaceuticals, and its derivatives were suggested as potent drugs.

The structure–activity relationship of Cin-amino acid Schiff bases (CAASBs) (Al-Resayes et al., 2016; Zhang et al., 2013) and some of their biological properties have been investigated (Nanda et al., 2015; Wang et al., 2017; Wang et al., 2016; Wei et al., 2011). The contributions of the benzene ring, carboxylic, and azomethine groups to bioactivity have also been reported (Wang et al., 2017; Wang et al., 2016). Meanwhile, no reports evaluating their hemolytic activity on erythrocytes have been published. Furthermore, their detailed structure was not adequately investigated. In this context, human erythrocytes provide a useful tool for studies of hemolytic activity, as an alternative to an *in vivo* test, thus reducing the use of laboratory animals. Hemolytic assay is an easy, rapid, reproducible, inexpensive, and effective method for assessing cellular toxicity (Greco et al., 2020). Substances might have a hemolytic or anti-hemolytic effect on human erythrocytes that necessitates practical research before their use. Furthermore, the development of bioactive compounds to control infectious diseases is a major healthcare challenge because of the emergence and dissemination of multidrug-resistant bacteria. Therefore, the discovery and development of novel antibiotics are particularly notable scientific achievements.

To the best of our knowledge, no research has been conducted on the hemolytic activity of N-(cinnamylidene)tryptophan, to assess its cellular toxicity. Moreover, its physicochemical, spectral, thermal, and biological properties have been inadequately reported. In this context, the objective of this study was to investigate the bioactivity, including cellular toxicity, as well as the physicochemical, spectral, and thermal properties, of CinTrp.

2. Materials and methods

2.1. Materials

Cin (98%), Trp (98%), potassium hydroxide (KOH, 99.9%), dimethyl sulfoxide (DMSO, 99.7%), phosphate-buffered saline (PBS, pH 7.4), and Triton X-100 (TX100, 0.1% v/v) were purchased from Sigma-Aldrich (Taufkirchen, Germany). Absolute ethanol was obtained from Fluka (St. Gallen, Switzerland). All other reagents were of analytical grade and were used as received without any further treatment.

2.2. Instruments

FTIR spectra were recorded by a Nicolet iS10 spectrophotometer (Thermo-Scientific, WI, USA), with an attenuated total reflection (ATR) accessory. The ^{1}H- and ^{13}C NMR spectra were obtained on a JEOL Delta-NMR spectrometer (JOEL Resonance, Tokyo, Japan) at 400 MHz, using DMSO d_6 as the solvent. The electronic spectra were recorded in ethanol using a U-2910 UV–Vis spectrophotometer (Hitachi, Tokyo, Japan) over the range of 200–500 nm. Mass spectra were obtained using an Accu-TOF LC-Plus JMS-T100 LP, ToF-MS (JEOL) operated in the +ve-ion mode. TGA analysis was performed on a Mettler-Toledo TGA/DSC 1 Star system (Columbus,

OH, USA), 7–12 mg, from 25 °C to 800 °C, at 10 °C/min, under an N_2 gas stream of 20 mL/min. DSC thermograms were acquired on a Shimadzu DSC60A (Kyoto, Japan). Samples ($\sim$10 mg) were heated from room temperature to 350 °C at a heating rate of 20 °C/min under an N_2 atmosphere (50 mL/min).

2.3. Synthesis of CinTrp

CinTrp Schiff base was synthesized via a condensation reaction between Cin (aldehyde) and Trp (primary amine) as described elsewhere (Wang et al., 2016). Typically, Trp (1.0 g, 5 mmol) was dissolved in 100 mL of a hot KOH (0.28 g, 5 mmol) ethanolic solution by stirring. To this solution, equimolar Cin (0.650 g) in 100 mL of hot ethanol was added dropwisely, stirred at room temperature for 2 h, then concentrated under a vacuum at 30 °C. The CinTrp precipitate was obtained by adding 25 mL diethyl ether, then filtered, washed three times with diethyl ether, dried at room temperature for 2 days, and stored in a vacuum desiccator until use.

2.4. Biological studies

2.4.1. Antibacterial activity tests

The *in vitro* antibacterial activity of CinTrp was determined by screening against Gram-positive (*S. aureus*) and Gram-negative (*E. coli*, *P. aeruginosa*, and *K. pneumoniae*) bacteria using the disk-diffusion method (Al-Qadsy et al., 2020; Azam et al., 2021b; Ommenya et al., 2020) in reference to ampicillin (Amp) and ceftriaxone (Cef). The test bacteria were kind gifts from Professor Fuad Al-Dubai (Thamar University), Thamar, Yemen. Nutrient agar (Himedia, Mumbai, India) was prepared in accordance with the manufacturer's directions and used to grow the bacteria. The test bacteria suspension was made to an inoculum density equivalent to 0.5 McFarland (approximately 1.5×10^8 CFU (colony-forming unit)/mL). The plates were inoculated with the target bacteria using sterilized cotton swabs. Sterile Whatman filter paper (No. 1) disks with a diameter of 6 mm were impregnated with different concentrations (20, 40, 100, 250, 500, 750, and 1000 μg/mL) of the CinTrp and positive controls (Cef and Amp) in DMSO; DMSO was also used as a negative control (Rehman et al., 2013). Subsequently, the impregnated disks were placed aseptically on the surface of bacterially seeded Petri dishes and immediately incubated at 37 °C for 18–24 h. The susceptibility of bacteria to CinTrp was determined by measuring the diameter of the inhibition zones (ZOI) in millimeters. All experiments were carried out in duplicate.

2.4.2. Hemolytic assay

An *in vitro* hemolytic activity test was carried out as described in the literature (Kumar et al., 2011). Five milliliters of blood were taken from a healthy individual (a 37-year-old male volunteer with an O-positive blood group) after the provision of informed consent and transferred into an EDTA-containing tube. The erythrocytes were isolated based on the procedure described by Chiste et al. (Chisté et al., 2014). Briefly, the blood was centrifuged at 1500 rpm for 5 min at 4 °C, followed by careful removal of the supernatant, washing the pellet five times with sterile PBS, and centrifuging using the same conditions. The cells were resuspended in PBS to obtain a 0.5% (v/v) erythrocyte suspension, which was subsequently used in the hemolysis assay. To each of nine marked test tubes containing 0.5 mL of the cell suspension, 0.5 mL of the following test samples were added: CinTrp solutions in sterile PBS, TX100 (positive control), and PBS (negative control). The tubes were incubated for 35 min at 37 °C and then centrifuged at 1500 rpm for 10 min at 4 °C to precipitate the cells. The obtained supernatant containing free hemoglobin was measured on a UV–Vis spectrophotometer at 540 nm. Sterile PBS and TX100 were used as minimal and maximal hemolytic controls, respectively. The level

Mohammed Mansour S. Saif, R.M. Alodeni, Abdulaziz Ali Alghamdi et al.

Journal of King Saud University – Science 34 (2022) 101988

of hemolysis caused by CinTrp was calculated according to Eq. (1), and the final hemolytic percentage was the average of three independent experiments.

$$Hemolysis(\%) = \left(\frac{A_t - A_n}{A_p - A_n}\right) \times 100, \qquad (1)$$

where A_t is the absorbance of the test sample, A_n is the absorbance of the negative control (PBS), and A_p is the absorbance of the positive control (TX100).

3. Results and discussion

3.1. Spectroscopic analysis of CinTrp

CinTrp or potassium 3-(1H-indol-3-yl)-2-(((E)-3-phenylallylidene)amino)propanoate) was synthesized as shown in Fig. S1 and its spectral (FTIR, ^{1}H-, ^{13}C NMR, UV–Vis, MS spectroscopy) and thermal (TGA/DTG and DSC) properties were discussed. CinTrp was obtained as a light-yellow powder, with an isolated yield of 93.26%.

3.1.1. FTIR analysis

The FTIR spectra of the CinTrp and its precursors are presented in Fig. 1, and the structural characteristic bands are listed in Table 1. The spectra of Cin and Trp typically accord with literature (Cao and Fischer, 1999; Wang et al., 2017). In the spectrum of Trp, the peaks at 3401 and 1356 cm^{-1}, assigned to the stretching and bending modes of N–H indole, are shifted to 3403 and 1371 cm^{-1}, respectively, in CinTrp. According to the literature (Cao and Fischer, 1999; Polfer et al., 2006), bands of NH$_2$ and NH^{3+}, expected in the region 3330–3030 cm^{-1} for stretching and at 1750–1650 cm^{-1} for bending modes, are commonly weak. However, the weak bands at 3077 and 3037 cm^{-1} and the strong ones at 1660 and 1144 cm^{-1} were assigned, respectively, to the asymmetric stretching, symmetric stretching, bending, and rocking vibrating modes of NH^{3+} moiety in Trp (Wagner and Baran, 2004). These bands were not observed in the spectrum of CinTrp, confirming amine transformation into imine. Moreover, the bands at 1582, 1410, and 741 cm^{-1} represented the carboxylic ion asymmetric stretching, symmetric stretching, and bending bands, respectively, which were observed at 1631, 1400, and 739 cm^{-1} in CinTrp. However, bands of carboxylate may overlap with that of the imine

Fig. 1. FTIR spectra of Cin, Trp, and the CinTrp Schiff base.

Table 1
FTIR characteristic bands of Cin, Trp, and CinTrp.

Peak Assignment	Trp (cm^{-1})	Cin (cm^{-1})	CinTrp (cm^{-1})
ν(N–H) indole	3401, vs	–	3404, w
ν_{asym}(NH$_3^+$); ν_{sym}(NH$_3^+$)	3077, m; 3037, m	–	–
ν(=CH)	3010–3037, m	3060–3028, m	3054–3026, w
ν(–CH)	2975–2847, w	–	2917–2872, w
ν(C–H, aldehyde)	–	2812, 2742, s	–
δ(NH$_3^+$)	1660, vs	–	
ν_{asym}(COO$^-$)	1582, vs	–	1631, s
ν(C=N, imine)	–	–	1579, vs
ν(HC=O)	–	1669, vs	–
ν(C=C) alkene	–	1625, vs	1489, s
ν(C=C) ring	1456, s	1449, vs	1455, s
ν_{sym}(C=O)	1410, vs	1392, m	1400, s
δ(C-N) indole	1356, vs	–	1371, s
δ(CH)	1315, m	1294, s	1293, m
τ(CH$_2$)	1230, s	–	1227, m
ρ(NH$_3^+$)	1144, s	–	–
ν(C-O)	–	1119, vs	–
ν(C-N) aliphatic	1098, s	–	1092, m
Ring deformation	1007–920, s	1006–921, s	1010–925, m
δ(COO$^-$)	741, vs	745, vs	739, vs

asym, asymmetric; sym, symmetric; w, weak; m, medium; s, strong; vs, very strong.

observed at 1579 cm^{-1}; that is, the alkali metal salt of an acidic compound commonly shows a red-shift of about 200 cm^{-1} due to transformation into carboxylate (Zhang et al., 2011). In the spectrum of Cin, peaks characterizing υ(C–H) of aldehyde at 2812 and 2742 cm^{-1} completely disappeared, confirming the success of the condensation reaction into CinTrp. The other peaks were assigned as shown in Table 1.

3.1.2. ^{1}H- and ^{13}C NMR

The ^{1}H- and ^{13}C NMR analyses of CinTrp are given in Fig. 2 and Table 2 (Trp and Cin spectra are provided in Figs. S2–S5). Inspection of the CinTrp ^{1}H NMR spectrum around the imine group revealed that the peak positions of –CH=N and –CH (No. 13 and 2, respectively) were shifted from 9.66 and 3.51 in, respectively, Cin and Trp to 7.55 and 3.80 ppm (Δppm are −2.11 and 0.29, respectively), because of the difference in the deshielding effect of oxygen and nitrogen. In addition, the integrated curves agreed with the number of hydrogens in the molecules (Fig. 2, S2–S5). The chemical shifts of most Trp-derived protons involved slight shifts downfield (+Δppm, see Table 2), but to upfield (−Δppm) for Cin-derived ones in CinTrp spectra. Likewise, in the ^{13}C NMR spectra of CinTrp, all carbons in the molecule are clearly identified (Fig. 2 and Table 2) with remarkable shifts in the carbon peak positions compared with the precursors. In addition, there was a large effect on the imine's adjacent carbons, namely, No. 13 and 2. Thus, the aldehyde-derived carbon (No. 13), which was observed at 194.54 ppm in Cin (C=O), was shifted to a lower frequency of 160.93 ppm (Δppm is −33.61) in the CinTrp spectrum (–CH=N) because of the variation in electronegativity of the oxygen and nitrogen atoms (Al-Odayni et al., 2019). For the same reason, Trp carbon No. 2 was shifted from 54.88 to 78.33 ppm (Δppm is 23.45) in CinTrp. Moreover, the chemical shifts corresponding to protons and 13-carbons of benzene rings are less affected, mostly due to their distance from the reaction center. All of the other protons and 13-carbons were assigned in Fig. 2, and S1–S4 and Table 2.

3.1.3. Mass analysis

The mass spectrum of CinTrp is shown in Fig. 3. The molecular ion expected at m/z 356 was not observed because of the low stability of the Schiff base, as suggested by thermal analysis (Al-Odayni et al., 2020). The fragmentation route is also schematically illustrated in Fig. 3, showing a relatively stable peak with an m/z of
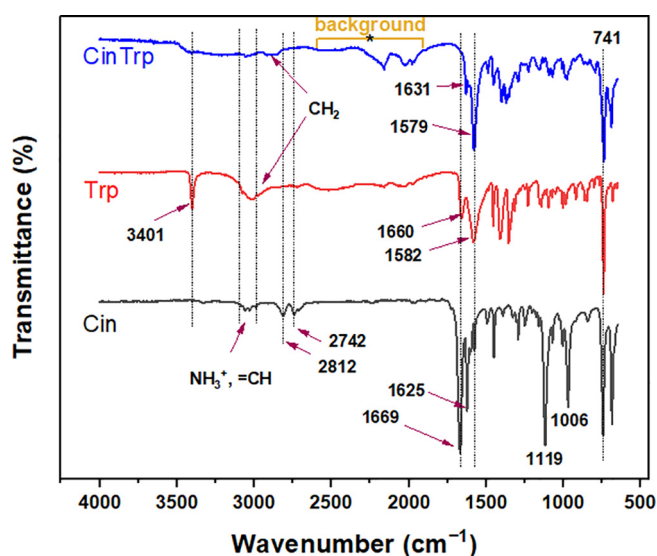
Mohammed Mansour S. Saif, R.M. Alodeni, Abdulaziz Ali Alghamdi et al.

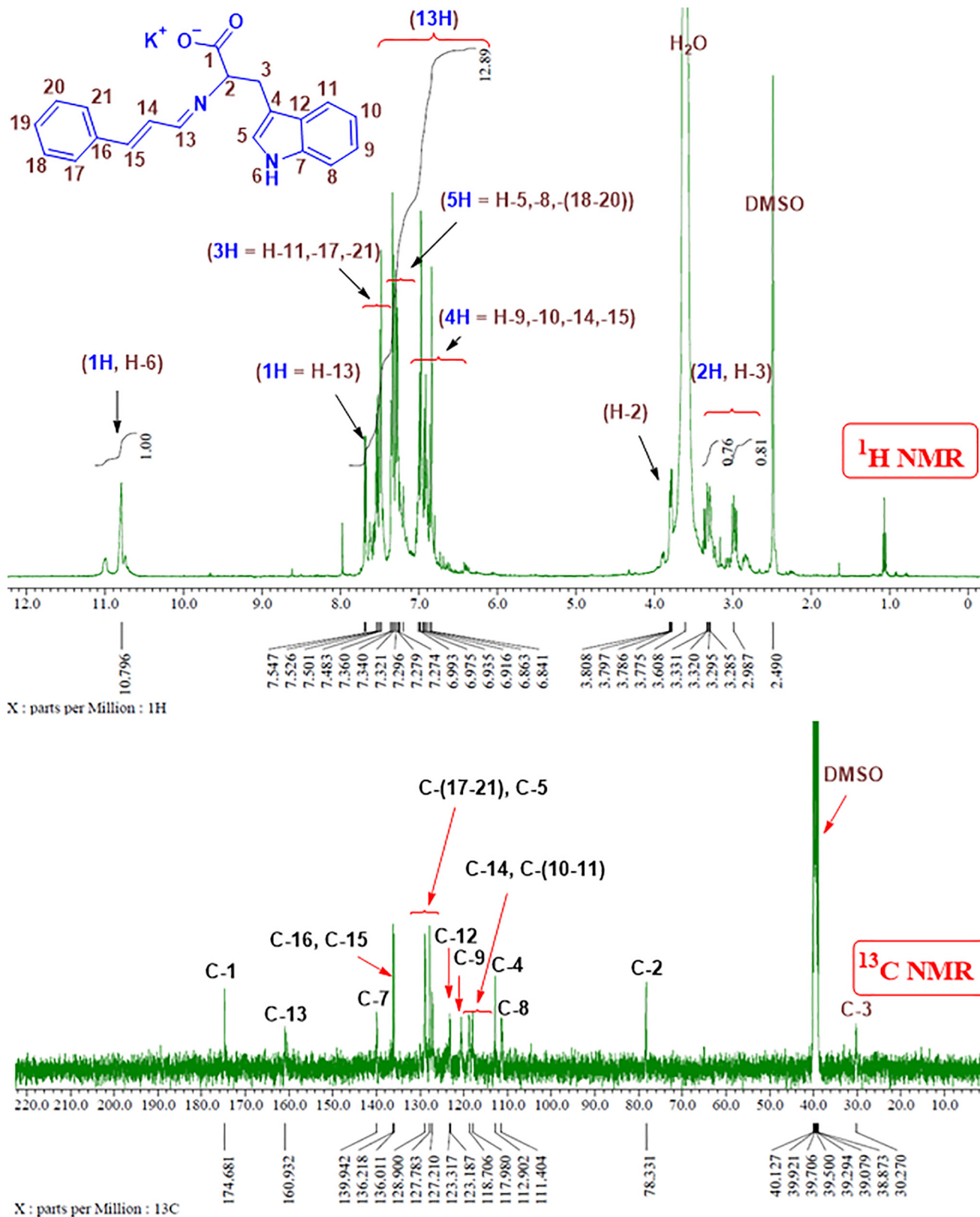Journal of King Saud University – Science 34 (2022) 101988

Fig. 2. ^{1}H NMR and ^{13}C NMR spectra of the CinTrp Schiff base in DMSO d_6.

275.15 (peak-B) assigned to COOK-truncated CinTrp. In this fragment, the presence of a C=N group indicates that the condensation reaction has taken place. The fragment with m/z of 549.30 (peak B-dimer) was assigned to the dimer of peak-B, possibly developed under fragmentation conditions. Other dimer-based fragments, for example, peak-A and peak-C, were also suggested. Fragment-A may undergo further ionization (i.e., to z = +2), providing a fragment with m/z of 248.14 (peak-A/2), which then decomposed into

Mohammed Mansour S. Saif, R.M. Alodeni, Abdulaziz Ali Alghamdi et al.

Journal of King Saud University – Science 34 (2022) 101988

Table 2
^{1}H- and ^{13}C NMR data for Trp, Cin, and CinTrp.

Position no.	^{1}H NMR (ppm)					^{13}C NMR (ppm)				
	Assig.	Trp	Cin	CinTrp	Δ (ppm)	Assig.	Trp	Cin	CinTrp	Δ (ppm)
1	–	–	–	–	–	C-1	170.60	–	174.68	4.08
2	H-2	3.51	–	3.80	0.29	C-2	54.88	–	78.33	23.45
3	2H, H-3	3.01, 3.31	–	3.30, 2.99	0.29, −0.32	C-3	27.19	–	30.27	3.08
4	–	–	–	–	–	C-4	109.51	–	112.90	3.39
5	H-5	7.23	–	7.36	0.13	C-5	124.43	–	123.32	−1.11
6	H-6	11.03	–	10.80	−0.23	–	–	–	–	–
7	–	–	–	–	–	C-7	136.52	–	139.94	3.42
8	H-8	7.35	–	7.34	−0.01	C-8	111.80	–	111.40	−0.40
9	H-9	7.03	–	6.94	−0.09	C-9	124.25	–	118.71	−5.54
10	H-10	6.98	–	6.92	−0.06	C-10	121.80	–	118.33	−3.47
11	H-11	7.60	–	7.53	−0.07	C-11	118.59	–	117.98	−0.61
12	–	–	–	–	–	C-12	127.39	–	123.19	−4.2
13	H-13	–	9.66	7.55	−2.11	C-13	–	194.54	160.93	−33.61
14	H-14	–	6.81	6.84	0.03	C-14	–	131.35	118.71	−12.64
15	H-15	–	7.68	6.86	−0.82	C-15	–	153.29	136.01	−17.28
16	–	–	–	–	–	C-16	–	134.15	136.22	2.07
17	H-17	–	7.68	7.50	−0.18	C-17	–	128.82	128.90–127.21	(−0.28)–(−1.32)
18	H-18	–	7.41	7.36	−0.05	C-18	–	129.18		
19	H-19	–	7.34	7.30	−0.04	C-19	–	128.53		
20	H-20	–	7.42	7.34	−0.08	C-20	–	129.18		
21	H-21	–	7.64	7.48	−0.16	C-21	–	128.82		

peak-C (Fig. 6). Overall, despite the absence of the molecular ion [M$^+$] in the fragmentation pattern, the results are consistent with the molecular structure of CinTrp as the observed peaks are all parts of its possible fragmentation.

3.1.4. UV–Vis analysis

Spectra of electronic transitions (UV–Vis) were practically recorded at a concentration of 6.3×10^{-5} M in absolute ethanol between 200 and 800 nm, as shown in Fig. 4 (only the range 200–500 is presented). The lowest wavelengths of the measurement are generally solvent-dependent; the cut-off limit for EtOH is 205 nm. In EtOH, two bands of Cin were clear at 286 (λmax, molar absorptivity (ε) = 29,492 M^{-1} cm^{-1}) and 219 nm. (Rind et al., 2011). Trp typically showed three overlapping peaks in the region between 240 and 310 nm, λmax of 280 nm and ε of 8206 M^{-1} cm^{-1} attributed to the π–π transition of aromatic rings; the peak at 272 nm was also assigned to the ring electronic transitions. The peak at 289 nm was attributed to the carboxylic functional group. The CinTrp profile was similar to that of Trp, with a small shift toward a higher wavelength (redshift, λ_{max} = 283 nm and ε = 26,539 M^{-1}.cm^{-1}). Moreover, peaks of the new azomethine (n–π*) could be detected in the lower-energy region, at about 304 and 340 nm (Al-Qadsy et al., 2021).

3.2. Thermal analysis

The DSC thermogram of CinTrp revealed only a decomposition-like profile (Fig. S6). However, a distinct drop above 200 °C and the presence of a small peak at 270 °C followed by a decomposition profile were observed, which led to the assumption of a melting point of 270 °C. The fusion of Trp was obtained as an exothermic peak at 292 °C. The TGA curves and the predicted decomposition steps are given in Fig. 5 and Table S1. The immediate decomposition of CinTrp indicated its lower thermal stability compared with that of Trp, with the loss of 4.3 wt% in the first stage assigned to adsorbed water and gases. The major mass loss of 63.7 wt% centered at DTG of 398 °C was assigned to the decomposition of the compound backbone, leaving a residue of about 33 wt% matching with five carbons and OK fragments. In this region, the low decomposition rate at the beginning may indicate gradual loss of CO_2 fragment first as suggested by mass profile and supported by the stabilized COOK-truncated mass fragment (peak-B, Fig. 3), fol-

lowed by backbone decomposition, the case that supposedly facilitated by the presence of the new azomethine and carboxylate groups. The mass loss of 6.0% above TGA 528 °C was due to the oxidation of unburnt carbons, a common occurrence at a higher temperature and under N_2 gas (Bernal et al., 2017). Conversely, three decomposition steps were observed for Trp. First, the mass loss of 16.2 wt% observed below 328 °C was attributed to NH_2 and OH. Second, a major mass loss was observed between 329 °C and 505 °C. Finally, heating above 600 °C left a mass residue of 18.7% assigned to residual carbons. The thermogram of Cin showed no decomposition profile; instead, a one-step, 100 wt% mass loss at 251 °C, close to its known melting point at 249 °C was observed; thus, under nitrogen gas, Cin undergoes no decomposition but evaporates before degradation.

3.3. Biological studies

3.3.1. Antibacterial activity

The antibacterial activity of CinTrp was determined using the paper disc method (Fig. S7). The data pertaining to the ZOI are listed in Table 3. CinTrp exhibited lower activity against all tested bacteria compared with the reference drugs, with no visible effect on *S. aureus* and *P. aeruginosa*. Conversely, moderate activity against *E. coli* and *K. pneumoniae* was observed, showing an almost equal ZOI value as that of Cef on the *E. coli* strain at 500 μg/mL. The ZOI value of Cef against *K. pneumoniae* was double that of CinTrp. However, in all cases, the inhibitory effect of Cef on the Gram-positive bacteria was more potent than that with CinTrp and Amp, while the effect of Amp on Gram-negative bacteria was stronger. Therefore, the lowest concentration of CinTrp that led to observable inhibition was 500 μg/mL, with no significant differences detected up to 1000 μg/mL. In a previous study evaluating the ZOI at the minimum inhibitory concentration (MIC) of 375 μg/mL of CinTrp and some other Cin-amino acid Schiff bases (Nanda et al., 2015), it was claimed that the ZOI of CinTrp against *E. coli* and *K. pneumoniae* was 2 and 0 mm, respectively. In the current work, both bacteria were found to be sensitive to CinTrp at 500 μg/mL, with higher activity against *E. coli* (Table 3). According to the literature, the resistance of bacteria to certain drugs is known to be associated with their surface chemistry (Manimaran et al., 2021), including hydrophobicity, as well as the type of transportation channels. Despite the lack of an outer cell membrane in
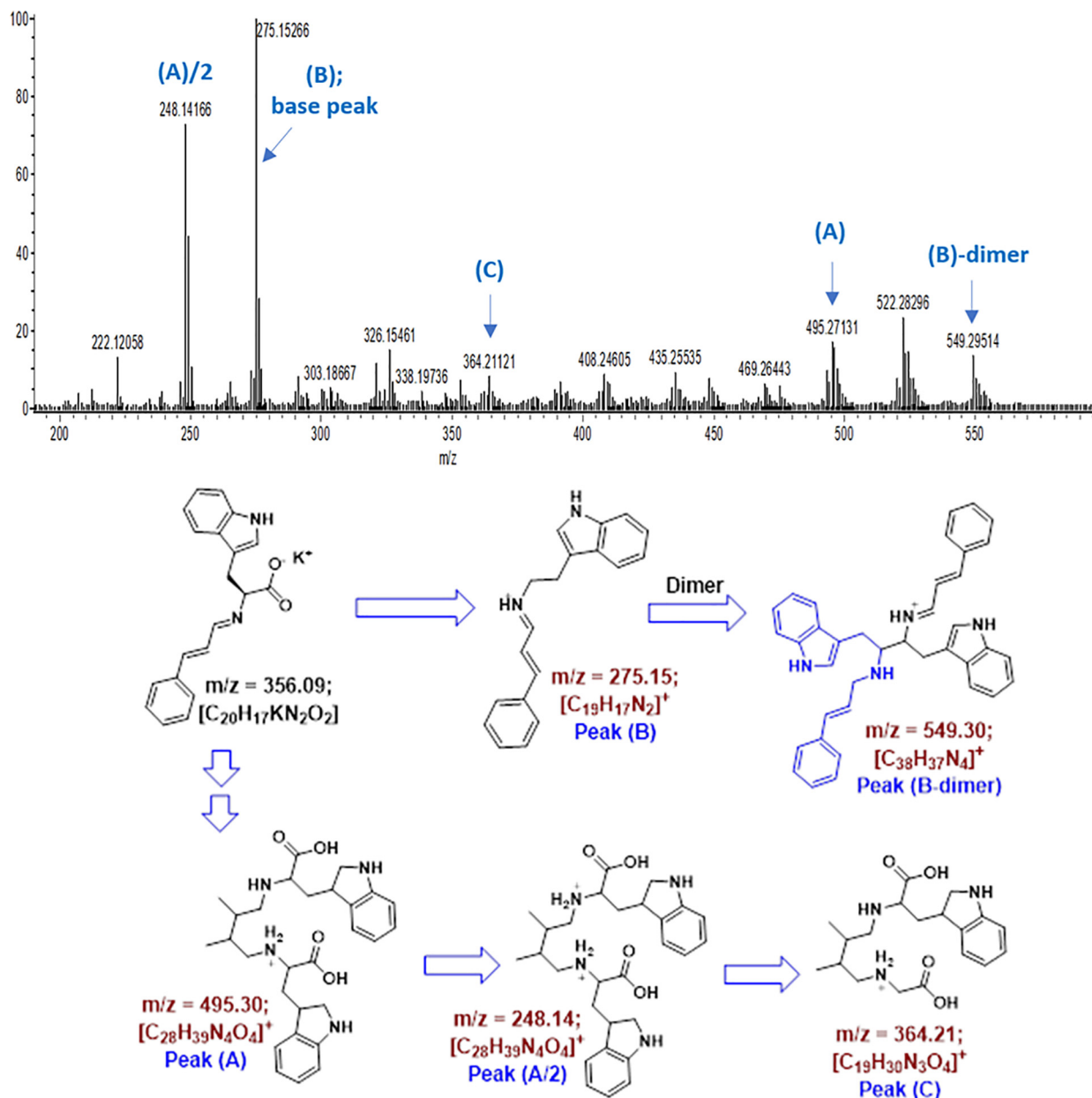
Mohammed Mansour S. Saif, R.M. Alodeni, Abdulaziz Ali Alghamdi et al.

Journal of King Saud University – Science 34 (2022) 101988

Fig. 3. Mass analysis of the CinTrp Schiff base.

Gram-positive bacteria, *S. aureus* has a more hydrophobic surface than *E. coli* (Lather et al., 2016; Mirani et al., 2018). The greater hydrophobicity of *S. aureus* as well as its thicker cell-wall and lack of an external surface membrane may contribute to its resistance to CinTrp (Oh et al., 2018). Furthermore, it seems that the structural properties of CinTrp enhance its interaction with Gram-negative bacteria, and thus increase its permeability, allowing its apparent activity against *E. coli* and *K. pneumoniae* (Wei et al., 2011); however, the mechanism of action involved requires further investigation.

3.3.2. Hemolytic activity

The hemolytic effect of the CinTrp assessed over the range of 20–1000 μg/mL on human red blood cells (hRBCs) under physiological conditions (pH 7.4 and 37 °C) was evaluated against PBS and TX100 as negative and positive controls, respectively (Fig. 6 and Table 4). Typically, erythrocytes provide a useful tool for toxicity studies as their membrane properties are well described and are easy to obtain. Practically, the results revealed a slight or no

hemolytic effect of CinTrp below 250 μg/mL (1.50%) compared with the 100% lysis of the TX100, with no significant differences up to 750 μg/mL (6.50%). However, a cell lysis of 23.13% at 1000 μg/mL was observed. Below 500 μg/mL, the effect was lower than the permissible range (<4.5%) (Bahojb Noruzi et al., 2020). Although dose-dependent hemolysis is a common observation, the mechanism underlying this phenomenon remains unclear; thus, necessitating further investigation before its biological utilization (Rahimi et al., 2017).

The biological activities of other CAASBs taken from literature are given in Table 5. The most relevant molecules with experimental conditions more closely resembling those of the CinTrp investigated here are presented for comparison. Wei et al. (Wei et al., 2011) studied the antibacterial activities of several amino acid-based Cin derivatives at concentrations of 200, 400, and 600 μg/mL against various bacterial strains, including *E. coli*. The reported ZOI values were the same (no inhibition against *P. aeruginosa*) or higher (against *E. coli* and *K. pneumoniae*) than those obtained by other researchers, such as Nanda et al. (Nanda
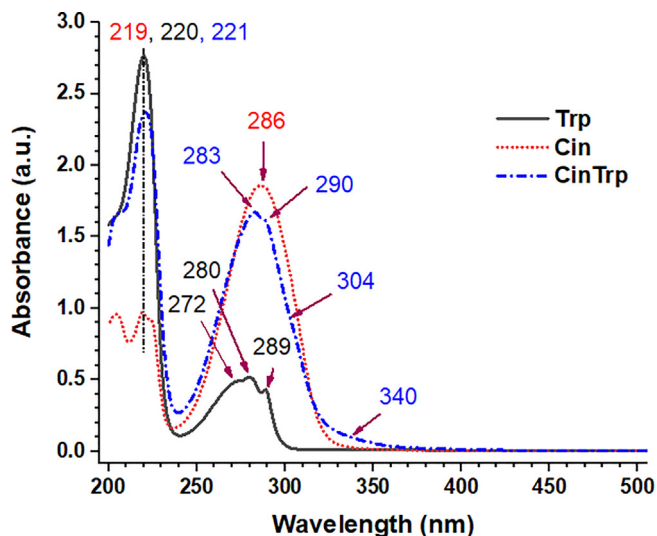
Mohammed Mansour S. Saif, R.M. Alodeni, Abdulaziz Ali Alghamdi et al.

Journal of King Saud University – Science 34 (2022) 101988

Fig. 4. UV–Vis spectra of Cin, Trp, and CinTrp (6.3×10^{-5} M) in ethanol.

et al., 2015); for instance, the ZOI value of CinTrp against *E. coli* obtained in this work (8.0 mm, 500 μg/mL) was in the acceptable region compared with the findings reported by Nanda (2.0 mm, 375 μg/mL). Wang et al. (Wang et al., 2016) reported the antibacterial activity of more than 24 Schiff base compounds of Cin and amino acids against *E. coli* and *S. aureus*; however, CinTrp was not included and the consistency with the results of other studies (Wei et al., 2011) is not clear, probably because of differences in the experimental conditions.

Conversely, because of the lack of reports on the hemolytic activity of Cin-amino acids in the literature, the comparison was difficult. Considering the Schiff base functional group, the hemolysis of 100 μg/mL of a curcumin-based Schiff base (Ali et al., 2013) yielded a hemolytic effect of about 21% (compared with letrazole, 100% lysis), while CinTrp at the same concentration yielded a hemolytic effect of 1.10% (compared with TX100, 100% lysis). However, the employed concentration range appeared to be high, resulting in an apparently toxic effect. Therefore, more extensive investigation may be important to draw a definitive conclusion on this issue.
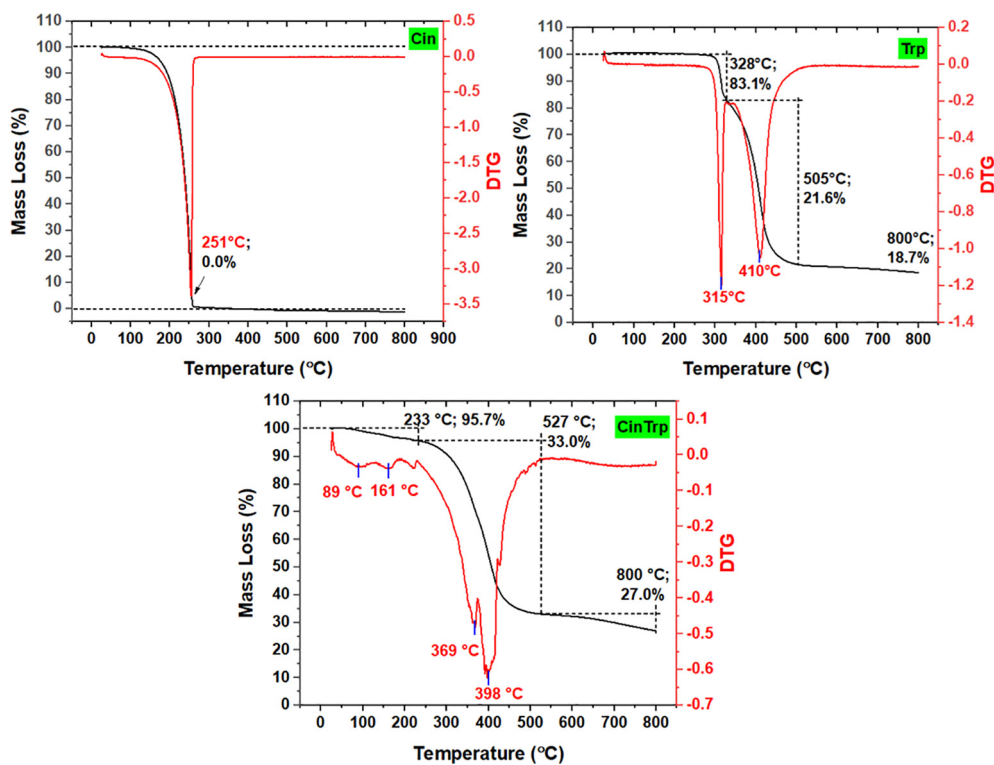

Fig. 5. TGA/DTG thermograms of cinnamaldehyde (Cin), tryptophan (Trp) and *N*-(cinnamylidene) tryptophan (CinTrp).

Table 3
Antibacterial activity of the CinTrp Schiff base.

Conc. (μg/mL)	Zone of Inhibition; mean and standard deviation (SD) (mm), (n = 2)											
	Gram-positive bacteria			Gram-negative bacteria								
	S. aureus			*E. coli*			*P. aeruginosa*			*K. pneumoniae*		
	CinTrp	Amp	Cef	CinTrp	Amp	Cef	CinTrp	Amp	Cef	CinTrp	Amp	Cef
20	–	–	21.5 (2.1)	–	–	–	–	–	–	–	–	–
40	–	–	26.0 (1.4)	–	7.5 (0.7)	–	–	–	–	–	–	–
100	–	–	29.5 (4.9)	–	10.3 (0.7)	–	–	8.3 (2.1)	–	–	8.0 (2.8)	7.5 (0.7)
250	–	10.0 (2.8)	34.0 (2.8)	–	14.5 (1.4)	–	–	12.5 (0.7)	–	–	12.0 (2.8)	10.0 (2.8)
500	–	13.5 (2.1	35.5 (3.5)	7.5 (0.7)	16.0 (0.0)	8.0 (0.0)	–	18.0 (0.0)	16.3 (2.1)	7.5 (0.7)	18.0 (2.8)	16.0 (0.0)
1000	–	18.3 (3.5)	39.5 (4.9)	7.5 (2.1)	18.0 (0.0)	9.5 (2.1)	–	19.5 (1.4)	18.5 (2.8)	8.0 (0.0)	23.5 (3.5)	18.5 (0.0)

Abbreviations: CinTrp, N-(cinnamylidene) tryptophan; Amp, ampicillin; Cef, ceftriaxone.
Notes: Dash sign (-) means no detection. Dimethyl sulfoxide (DMSO) used as a negative control showed no zone of inhibition. The values represent the average of two independent experiments with standard deviation (SD) given in bracket.
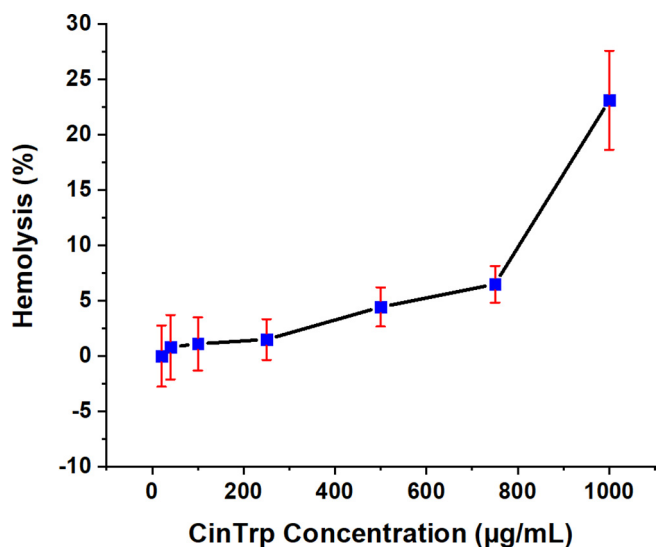
Fig. 6. Percentage of hemolysis of hRBCs caused by the CinTrp Schiff base under the test conditions. Data points are means, and bars represent the standard error of the mean (SeM) from triplicates.

4. Conclusion

To assess the physical, chemical, and biological properties of CinTrp, spectral, thermal, antibacterial, and hemolysis tests were performed. The structural properties of CinTrp were detailed using FTIR, ^{1}H-, ^{13}C NMR, UV–Vis, and MS analyses. The thermal analysis indicated a slightly lower stability of CinTrp than Trp. The *in vitro* antibacterial activity tests proved CinTrp selective potential activity against *E. coli* and *K. pneumoniae* compared with the findings for *S. aureus* above 250 μg/mL, in reference to Cef and Amp. In this case, its activity was as high as that of Cef throughout the concentration range. Conversely, *S. aureus* and *P. aeruginosa* were insensitive to CinTrp up to 1000 μg/mL. The hemolytic activity test, in reference to PBS and TX100 as negative and positive controls, respectively, revealed negligible effects (<1.5%) below 250 μg/mL, and as low as 6.5% at 750 μg/mL. However, a hemolytic value of 23.13% was detected at 1000 μg/mL. Consequently, it could be concluded that CinTrp is more active against *E. coli* and its hemocompatibility at moderate concentrations, below 500 μg/mL, on hRBCs is permissible. These findings might be useful in terms of developing pharmaceutical products and thus warrant further intensive investigation.

Declaration of Competing Interest

The authors declare that they have no known competing financial interests or personal relationships that could have appeared to influence the work reported in this paper.

Table 4
Hemolytic activity of the *N*-(cinnamylidene)tryptophan Schiff base on human erythrocyte cells.

Hemolysis; mean and standard deviation (SD) (%), (n = 3)								
Controls		*N*-(cinnamylidene)tryptophan concentration (μg/mL)						
Triton X-100 (0.1% v/v) (positive control)	Phosphate-buffered saline (negative control)	20	40	100	250	500	750	1000
100.00 (7.80)	0.00 (2.91)	0.01 (4.81)	0.81 (5.03)	1.10 (4.18)	1.50 (3.20)	4.43 (3.06)	6.50 (2.87)	23.13 (7.76)

Values represent the average of three independent experiments (n = 3) with standard deviation (SD) given in bracket.

Table 5
Comparison of the bacterial activity of some cinnamaldehyde amino acid Schiff bases taken from the literature.

Cin-amino acid SB	Bacteria; method; Standard; Ref.	Conc. (μg/mL) (*)	ZOI (mm) (**)
CinGly	*E. coli*;	200 (600)	14.2 (21.8)
CinAla	diffusion disk;Cin. (5.5)	200 (600)	14.3 (22.4)
CinVal	,Benzene (3.5)	200 (600)	13.1 (20.3)
CinPhe	;	200 (600)	14.1 (21.3)
CinLeu	(Wei et al., 2011)	200 (600)	14.3 (21.3)
CinGlu		200 (600)	13.4 (20.8)
CinAsp		200 (600)	13.1 (20.6)
CinGln		200 (600)	13.3 (21.5)
CinMet		200 (600)	13.5 (21.9)
CinTrp	*E. coli*; diffusion disk; amoxicillin, doxycycline MIC of both is 10 μg/mL (Nanda et al., 2015)	375	2
	K. pneumoniae; diffusion disk; amoxicillin, doxycycline MIC of both is 10 μg/mL (Nanda et al., 2015)	375	–
CinHis	*E. coli*; diffusion disk; amoxicillin, doxycycline MIC of both is 10 μg/mL (Nanda et al., 2015)	250	–
	K. pneumoniae; diffusion disk; amoxicillin, doxycycline MIC of both is 10 μg/mL (Nanda et al., 2015)	250	–
CinPhe	*E. coli*; diffusion disk; Cin (8.0), ciprofloxacin (22.3) (Wang et al., 2016)	9523 (0.03 mol/L)	8.0
	S. aureus; diffusion disk; Cin (8.0), ciprofloxacin (16.0) (Wang et al., 2016)	9523 (0.03 mol/L)	10.0

Abbreviations: ZOI, zone of inhibition; MIC, minimum inhibitory concentration; SB, Schiff base; Gly, glycine; Ala, alanine; Val, valine; Phe, phenylalanine; Leu, leucine; Glu, glutamic acid; Asp, aspartic acid; Gln, glutamine; Met, methionine; His, histidine. (*) indicates another concentration (Conc.) used and (**) its ZOI value.

Appendix A. Supplementary data

Supplementary data to this article can be found online at https://doi.org/10.1016/j.jksus.2022.101988.

References

Adabiardakani, A., Mohammad, H., Kargar, H., 2012. Cinnamaldehyde schiff base derivatives: a short review. World Appl. Program 2, 472–476.

Al-Odayni, A.-B., Alfotawi, R., Khan, R., Sharaf Saeed, W., Al-Kahtani, A., Aouak, T., Alrahlah, A., 2019. Synthesis of chemically modified BisGMA analog with low viscosity and potential physical and biological properties for dental resin composite. Dent. Mater. 35 (11), 1532–1544.

Al-Odayni, A.-B., Saeed, W.S., Ahmed, A.Y.B.H., Alrahlah, A., Al-Kahtani, A., Aouak, T., 2020. New monomer based on eugenol methacrylate, synthesis, polymerization and copolymerization with methyl methacrylate-characterization and thermal properties. Polymers 12, 160.

Al-Qadsy, I., Saeed, W.S., Al-Odayni, A.-B., Saeed, W.S., Alrabie, A., Al-Adhreai, A., Al-Faqeeh, L.A.S., Lama, P., Alghamdi, A.A., Farooqui, M., 2021. Synthesis, characterization, single-crystal X-ray structure and biological activities of [(Z)-N′-(4-Methoxybenzylidene) benzohydrazide–nickel (II)] complex. Crystals 11, 110.

Al-Qadsy, I., Saeed, W.S., Al-Odayni, A.-B., Ahmed Saleh Al-Faqeeh, L., Alghamdi, A. A., Farooqui, M., 2020. Novel metformin-based schiff bases: synthesis, characterization, and antibacterial evaluation. Materials 13 (3), 514.

Al-Resayes, S.I., Azam, M., Trzesowska-Kruszynska, A., Kruszynski, R., Soliman, S.M., Mohapatra, R.K., Khan, Z., 2020. Structural and theoretical investigations, Hirshfeld surface analyses, and cytotoxicity of a naphthalene-based chiral compound. ACS Omega 5 (42), 27227–27234.

Al-Resayes, S.I., Shakir, M., Shahid, N., Azam, M., Khan, A.U., 2016. Synthesis, spectroscopic characterization and in vitro antimicrobial studies of Schiff base ligand, H2L derived from glyoxalic acid and 1, 8-diaminonaphthalene and its Co (II), Ni (II), Cu (II) and Zn (II) complexes. Arab. J. Chem. 9 (3), 335–343.

Alam, M.S., Choi, J.-H., Lee, D.-U., 2012. Synthesis of novel Schiff base analogues of 4-amino-1, 5-dimethyl-2-phenylpyrazol-3-one and their evaluation for antioxidant and anti-inflammatory activity. Bioorg. Med. Chem. 20 (13), 4103–4108.

Ali, I., Saleem, K., Wesselinova, D., Haque, A., 2013. Synthesis, DNA binding, hemolytic, and anti-cancer assays of curcumin I-based ligands and their ruthenium (III) complexes. Med. Chem. Res. 22 (3), 1386–1398.

Azam, M., Wabaidur, S.M., Alam, M., Khan, Z., Alanazi, I.O., Al-Resayes, S.I., Moon, I. S., Rajendra, 2021a. Synthesis, characterization, cytotoxicity, and molecular docking studies of ampyrone-based transition metal complexes. Trans. Met. Chem. 46 (1), 65–71.

Azam, M., Wabaidur, S.M., Alam, M., Trzesowska-Kruszynska, A., Kruszynski, R., Al-Resayes, S.I., Alqahtani, F.F., Khan, M.R., 2021b. Design, structural investigations and antimicrobial activity of pyrazole nucleating copper and zinc complexes. Polyhedron 195.

Bahojb Noruzi, E., Shaabani, B., Geremia, S., Hickey, N., Nitti, P., Kafil, H.S., 2020. Synthesis, crystal structure, and biological activity of a multidentate calix [4] arene ligand doubly functionalized by 2-hydroxybenzeledene-thiosemicarbazone. Molecules 25, 370.

Bernal, S.A., Juenger, M.C., Ke, X., Matthes, W., Lothenbach, B., De Belie, N., Provis, J. L., 2017. Characterization of supplementary cementitious materials by thermal analysis. Mater. Struct. 50, 1–13.

Cao, X., Fischer, G., 1999. Infrared spectral, structural, and conformational studies of zwitterionic L-tryptophan. J. Phys. Chem. A 103, 9995–10003.

Chisté, R.C., Freitas, M., Mercadante, A.Z., Fernandes, E., 2014. Carotenoids inhibit lipid peroxidation and hemoglobin oxidation, but not the depletion of glutathione induced by ROS in human erythrocytes. Life Sci. 99 (1-2), 52–60.

da Nóbrega Alves, D., Monteiro, A.F.M., Andrade, P.N., Lazarini, J.G., Abílio, G.M.F., Guerra, F.Q.S., Scotti, M.T., Scotti, L., Rosalen, P.L., Castro, R.D.D., 2020. Docking prediction, antifungal activity, anti-biofilm effects on Candida spp., and toxicity against human cells of cinnamaldehyde. Molecules 25, 5969.

Greco, I., Molchanova, N., Holmedal, E., Jenssen, H., Hummel, B.D., Watts, J.L., Håkansson, J., Hansen, P.R., Svenson, J., 2020. Correlation between hemolytic activity, cytotoxicity and systemic in vivo toxicity of synthetic antimicrobial peptides. Sci. Rep. 10.

Khan, T., Azad, I., Ahmad, R., Lawrence, A.J., Azam, M., Wabaidur, S.M., Al-Resayes, S. I., Raza, S., Khan, A.R., 2021. Molecular structure simulation of (E)-2-(butan-2-ylidene) hydrazinecarbothioamide using the DFT approach, and antioxidant potential assessment of its complexes. J. King Saud Univ.-Sci. 33, 101313.

Kumar, G., Karthik, L., Rao, K.V.B., 2011. Hemolytic activity of Indian medicinal plants towards human erythrocytes: an in vitro study. Elixir. Appl. Botany 40, 5534–5537.

Lather, P., Mohanty, A.K., Jha, P., Garsa, A.K., 2016. Contribution of cell surface hydrophobicity in the resistance of Staphylococcus aureus against antimicrobial agents. Biochem. Res. Int. 2016, 1–5.

Li, S., Freitag, C., Morrell, J.J., 2008. Preventing fungal attack of freshly sawn lumber using cinnamon extracts. Forest Products Journal 58, 77–82.

Manimaran, P., Balasubramaniyan, S., Azam, M., Rajadurai, D., Al-Resayes, S.I., Mathubala, G., Manikandan, A., Muthupandi, S., Tabassum, Z., Khan, I., 2021. Synthesis, spectral characterization and biological activities of Co (II) and Ni (II) mixed ligand complexes. Molecules 26, 823.

Mirani, Z.A., Fatima, A., Urooj, S., Aziz, M., Khan, M.N., Abbas, T., 2018. Relationship of cell surface hydrophobicity with biofilm formation and growth rate: A study on Pseudomonas aeruginosa, Staphylococcus aureus, and Escherichia coli. Iran. J. Basic Med. Sci. 21, 760.

Nanda, R., Nainawat, K.S., Chitlange, S.S., Hatolar, S., 2015. Design, synthesis and biological evaluation of caffeic acid analogue for peptide deformylase based antimicrobial activity. Asian J. Biomed. Pharmaceut. Sci. 5, 16.

Oh, J.K., Yegin, Y., Yang, F., Zhang, M., Li, J., Huang, S., Verkhoturov, S.V., Schweikert, E.A., Perez-Lewis, K., Scholar, E.A., Taylor, T.M., Castillo, A., Cisneros-Zevallos, L., Min, Y., Akbulut, M., 2018. The influence of surface chemistry on the kinetics and thermodynamics of bacterial adhesion. Sci. Rep. 8 (1).

Ommenya, F.K., Nyawade, E.A., Andala, D.M., Kinyua, J., 2020. Synthesis, characterization and antibacterial activity of schiff base, 4-chloro-2-{(E)-[(4-Fluorophenyl)imino]methyl}phenol metal (II) complexes. J. Chem. 2020, 1–8.

Polfer, N.C., Oomens, J., Dunbar, R.C., 2006. IRMPD spectroscopy of metal-ion/ tryptophan complexes. PCCP 8, 2744–2751.

Rahimi, M., Shojaei, S., Safa, K.D., Ghasemi, Z., Salehi, R., Yousefi, B., Shafiei-Irannejad, V., 2017. Biocompatible magnetic tris (2-aminoethyl) amine functionalized nanocrystalline cellulose as a novel nanocarrier for anticancer drug delivery of methotrexate. New J. Chem. 41 (5), 2160–2168.

Rehman, M., Imran, M., Arif, M., 2013. Synthesis, Characterization and in vitro Antimicrobial studies of Schiff-bases derived from Acetylacetone and amino acids and their oxovanadium (IV) complexes. Am. J. Appl. Chem. 1, 59–66.

Rind, F., Memon, A., Almani, F., Laghari, M., Mughal, U., Maheshwari, M., Khuhawar, M., 2011. Spectrophotometric determination of cinnamaldehyde from crude drugs and herbal preparations. Asian J. Chem. 23, 631–635.

Shakir, M., Shahid, N., Sami, N., Azam, M., Khan, A.U., 2011. Synthesis, spectroscopic characterization and comparative DNA binding studies of Schiff base complexes derived from l-leucine and glyoxal. Spectrochim. Acta Part A Mol. Biomol. Spectrosc. 82 (1), 31–36.

Shreaz, S., Sheikh, R.A., Bhatia, R., Neelofar, K., Imran, S., Hashmi, A.A., Manzoor, N., Basir, S.F., Khan, L.A., 2011. Antifungal activity of α-methyl trans cinnamaldehyde, its ligand and metal complexes: promising growth and ergosterol inhibitors. Biometals 24 (5), 923–933.

Wagner, C.C., Baran, E.J., 2004. Spectroscopic and magnetic behaviour of the copper (II) complex of L-tryptophan. Acta Farm. Bonaerense 23, 339–342.

Wang, H., Jiang, M., Li, S., Hse, C.-Y., Jin, C., Sun, F., Li, Z., 2017. Design of cinnamaldehyde amino acid Schiff base compounds based on the quantitative structure–activity relationship. Royal Soc. Open Sci. 4, 170516.

Wang, H., Jiang, M., Sun, F., Li, S., Hse, C.-Y., Jin, C., 2018. Screening, synthesis, and QSAR research on cinnamaldehyde-amino acid Schiff base compounds as antibacterial agents. Molecules 23, 3027.

Wang, H., Yuan, H., Li, S., Li, Z., Jiang, M., 2016. Synthesis, antimicrobial activity of Schiff base compounds of cinnamaldehyde and amino acids. Bioorg. Med. Chem. Lett. 26 (3), 809–813.

Wei, Q.-Y., Xiong, J.-J., Jiang, H., Zhang, C., Ye, W., 2011. The antimicrobial activities of the cinnamaldehyde adducts with amino acids. Int. J. Food Microbiol. 150, 164–170.

Zhang, H.-J., Qin, X., Liu, K., Zhu, D.-D., Wang, X.-M., Zhu, H.-L., 2011. Synthesis, antibacterial activities and molecular docking studies of Schiff bases derived from N-(2/4-benzaldehyde-amino) phenyl-N′-phenyl-thiourea. Bioorg. Med. Chem. 19 (18), 5708–5715.

Zhang, Y., Li, S., Kong, X., 2013. Relationship between antimold activity and molecular structure of cinnamaldehyde analogues. Bioorg. Med. Chem. Lett. 23 (5), 1358–1364.

Zong Chin, K., May Lee, L., Irene, L., 2020. Synthesis and anti-bacterial properties of Schiff bases and Schiff base copper (II) complexes derived from cinnamaldehyde and different hydrazides. J. Trans. Metal Complex.